


Article

Measurement of Diurnal Variation in Needle PRI and Shoot Photosynthesis in a Boreal Forest

Matti Mõttus ^{1,*} , Rocío Hernández-Clemente ², Viljami Perheentupa ³, Vincent Markiet ^{1,3}, Juho Aalto ^{4,5}, Jaana Bäck ⁶ and Caroline J. Nichol ⁷

¹ VTT Technical Research Centre of Finland, P.O. Box 1000, FI-02044 Espoo, Finland; vincent.markiet@vtt.fi

² Department of Geography, Swansea University, Swansea SA2 8PP, UK; r.hernandez-clemente@swansea.ac.uk

³ Department of Geosciences and Geography, University of Helsinki, P.O. Box 68, FI-00014 Helsinki, Finland; viljami.perheentupa@live.fi

⁴ SMEAR II Station, Hyytiälä Forestry Field Station, Hyytiäläntie 124, FI-35500 Helsinki, Finland; juho.aalto@helsinki.fi

⁵ Department of Physics, University of Helsinki, FI-00014 Helsinki, Finland

⁶ Department of Forest Sciences, University of Helsinki, P.O. Box 27, FI-00014 Helsinki, Finland; jaana.back@helsinki.fi

⁷ School of GeoSciences, University of Edinburgh, Alexander Crum Brown Road, Edinburgh EH9 3FF, UK; Caroline.Nichol@ed.ac.uk

* Correspondence: matti.mottus@gmail.com; Tel.: +358-40-849-3037

Received: 15 May 2018; Accepted: 23 June 2018; Published: 26 June 2018



Abstract: The photochemical reflectance index (PRI) is calculated from vegetation narrowband reflectance in two bands in the visible part of the spectrum. Variations in PRI are associated with changes in the xanthophyll cycle pigments which regulate the light use efficiency of vegetation. Correlations have been found between remotely-sensed PRI and various photosynthetic productivity parameters at the scales from leaves to landscapes. Environmental satellites can provide only an instantaneous value of this index at the time of overpass. The diurnal course of needle (leaf) PRI needs to be known in order to link the instantaneous values robustly with photosynthetic parameters at time scales exceeding one day. This information is not currently available in the scientific literature. Here we present the daily cycle of Scots pine needle and canopy PRI in a southern boreal forest zone in the presence of direct solar radiation during the peak growing season of two consecutive years. We found the PRI of the needles which are exposed to direct radiation to have a distinct diurnal cycle with constant or slightly increasing values before noon and a daily minimum in the afternoon. The cycle in needle PRI was not correlated with that in the incident photosynthetic photon flux density (PPFD). However, when PPFD was above $1000 \mu\text{mol m}^{-2} \text{s}^{-1}$, approximately between 8 a.m. and 5 p.m., needle PRI was correlated with the light use efficiency (LUE), measured with shoot chambers. The timing of the minimum needle PRI coincided with the minimum canopy value, as measured by an independent sensor above the canopy, but the correlation between the two variables was not significant. Our field results corroborate the applicability of needle PRI in monitoring the daily variation in LUE. However, to apply this to remote sensing of seasonal photosynthetic productivity, the daily cycle of leaf PRI needs to be known for the specific vegetation type.

Keywords: photochemical reflectance index; light use efficiency; gross primary production; shoot chamber; *Pinus sylvestris*; Scots pine

1. Introduction

Successful quantification of the terrestrial carbon cycle requires determination of the efficiency with which the absorbed photosynthetically active radiation (PAR) is utilized in the fixation of carbon by plants [1,2]. This efficiency, known as the light use efficiency (LUE), depends on the amount of vegetation cover and is constrained by various environmental factors, such as temperature and the availability of water. Commonly, the constraints are inferred from climatological or meteorological data. However, remote sensing of LUE, or its variations with time, could improve global estimations of photosynthetic productivity [1].

Although many unresolved issues exist, a potential tool for achieving this is the photochemical reflectance index (PRI) [3,4], a narrowband spectral index which can be easily calculated from remotely sensed data. It is defined as follows [5]:

$$\text{PRI} = \frac{R(531) - R(570)}{R(531) + R(570)} \quad (1)$$

where $R(\lambda)$ is the reflectance at the wavelength λ given in nanometers. PRI depends explicitly on the fraction of absorbed PAR that is dissipated as heat [6] and its use has been shown to improve the estimates of carbon fluxes in leaves and canopies using remotely-sensed data [7,8]. Recently, the power of this index has been demonstrated empirically using MODIS ocean band 11 (526–536 nm) [9,10] and has been shown to be a useful proxy for tracking phenology in the boreal ecosystem [10]. MODIS is currently the only space-based instrument which is providing global data in this spectral region on a near daily basis. Although MODIS lacks the reference band at 570 nm, it has been demonstrated that other spectral channels have been successfully used [9,11,12], for example, those at 551 and 667 nm. Furthermore, hyperspectral missions which fully satisfy the spectral requirements for calculating PRI are under preparation at the ESA [6] and NASA [13].

Two types of leaf PRI changes with time can be distinguished [14–16]: constitutive and facultative ones. Constitutive changes, also referred to as sustainable, occur on a time scale of weeks to months and are associated with pigment pools [17,18]. The reversible facultative changes are caused by the interconversion of xanthophyll cycle pigments [15] and occur on time scales from seconds to hours. Due to the involvement of xanthophylls in non-photosynthetic quenching of absorbed PAR, facultative PRI changes are directly related to LUE. The link between PRI and LUE, therefore, provides an opportunity to improve the mapping of carbon sequestration by vegetation from remote sensing data. The processes involved are extensively documented in the literature and the reader is referred to Garbulsky et al. [7] and Alonso et al. [19].

Earth observation satellites are mostly in sun-synchronous orbits and revisit each location at a specific and constant local time. The power of satellite-measured PRI in measuring terrestrial photosynthesis, compared with other narrowband spectral indices, lies in its ability to capture dynamic changes in LUE. However, to relate remotely-detected changes in instantaneous photosynthetic downregulation to changes in daily or seasonal productivity, the daily baseline curve for PRI (or, equivalently, LUE) is one of the variables that needs to be known for the observed vegetation type. The need to take into account the daily cycle of forest PRI for an improved remote estimate of LUE was recently demonstrated using the two satellites with the MODIS sensor on Aqua and Terra, with different overpass times [9]. The remotely-sensed PRI values corresponding to a specific vegetation type is strongly affected by vegetation structure, observation geometry and the spectral composition of diffuse sky radiation [9,20–25] and, hence, not direct measures of leaf PRI. In a boreal forest, canopy structure does not change on a daily time scale, but illumination geometry and the spectral composition of incident radiation (caused by the varying fraction of diffuse sky radiation dominated by shorter wavelengths) does vary with the solar angle continuously on a clear day. These non-physiological variations need to be removed before canopy PRI measurements made at different times of day can be compared. Measurements of leaf PRI daily curves are, therefore, necessary to

validate the algorithms for removing the non-physiological PRI components. Currently, information on the daily cycle of leaf-level PRI in natural environments is limited.

In the present study, we provide the first account of the diurnal cycle of needle PRI in a boreal Scots pine stand, under natural illumination, and its relationship with primary productivity. The aim of the research was to assess the potential of instantaneous measurements of canopy PRI for monitoring the photosynthesis of a boreal conifer forest.

2. Materials and Methods

2.1. Needle Optical Measurements

Two spectral measurement campaigns were carried out in a boreal coniferous forest at the Station for Measuring Ecosystem Atmosphere Relationships (SMEAR II) in Hyytiälä, Southern Finland (61°51'N, 24°18'E) in 2014 and 2015. The growing season in this area, determined as the period for which mean temperature is above 5 °C, lasts between late April and October [26]. The site is located on mineral soils and dominated by Scots pine (*Pinus sylvestris* L.) and Norway spruce (*Picea abies* (L.) Karst), with forest understory consisting of common vascular plant species [27].

The campaigns were carried out during the peak growing season, on 24–25 July 2014, and 1–5 July 2015. During the short July 2014 campaign all measurements were carried out within 24 h. Illumination conditions were clear with cumulus clouds only very occasionally interrupting the measurements in the afternoon. During the 2015 campaign, we experienced both complete and broken cloud cover, and also a complete day with no clouds (3 July). The data recorded during the 2015 campaign were pooled to derive a daily cycle of the PRI of sunlit and shaded needles for the campaign period. The number of measurement campaigns was limited by weather: in this region, sunny days are infrequent—it is possible that only a few days during the peak growing period are suitable for daily PRI studies.

One mature (ca. 55 year-old) Scots pine (*Pinus sylvestris*) tree was sampled in 2014 and two trees in 2015. The measurements were performed in the upper crowns accessed using two walk-up scaffolding towers (18 m in height). We selected eight shoots in each tree at the beginning of each campaign. Four shoots were marked in the southern (sunlit) side of the crown, and four shoots in the northern (shaded) crown. While all shoots were located in the upper canopy layers visible to a remote sensing sensor, the shaded shoots were not exposed to direct sunlight for most of the day, especially before and around noon. Due to the high latitude, the shaded shoots received some direct sunlight late in the evening when the sun was in the northern part of the sky. The selection of the shoots was based on visual observations of the shoot location. Illumination conditions were validated using hemispherical photographs taken with a 180° fisheye lens in the location of the shoot. Camera orientation was determined using a compass and a bubble level in the flash shoe. We used the WSL Hemisfer (Birmensdorf, Switzerland) software to calculate the light regime for each shoot.

We only included fully-expanded needles from the previous year in the study. To measure the PRI of an individual needle, it was partly inserted into a PP Systems (Amesbury, MA, USA) UNI501 Mini Leaf Clip for a few seconds. A small (diameter approx. 1.5 mm) spot was illuminated on the sample by light arriving from an Ocean Optics (Dunedin, FL, USA) HL-2000 tungsten halogen light source (power 5 W). Light reflected backward was analysed with an Ocean Optics USB4000-VIS-NIR portable modular spectrometer controlled by a notebook computer running the OceanView (Ocean Optics, Dunedin, FL, USA) spectroscopy application. Low OH bifurcated optical cables (PP Systems item UNI410) were used to connect the light source, needle clip, and spectroradiometer. The spectral resolution of the spectrometer was 1.5–2.3 nm (full width half maximum, FWHM) inside the useable wavelength range of the system 400–900 nm. As a reference, a white Spectralon disc was measured after each of three (in 2014) or five (in 2015) needle spectra measurements. The recorded spectra were converted to reflectance factors and smoothed with a Savitzky-Golay filter with parameters chosen not to reduce the spectral resolution determined by the spectroradiometer. The photosynthetic photon flux density

(PPFD) received by the target was determined using the Spectralon measurements performed in the field. The approximate value was $600\text{--}700 \mu\text{mol m}^{-2} \text{s}^{-1}$, which constitutes approximately two-thirds of that on sunlit needle surfaces in Finland in midsummer. In 2014, the four shoots in either sunlit or shaded locations of each tree were measured in a rapid sequence without distinguishing between them. In 2015, the shoots were measured separately with 20 needles sampled per shoot. The time required for measuring one shoot was approximately from four to six minutes. For each measurement, we calculated the average PRI and, assuming a normal distribution, its 90% confidence interval.

We calculated the PRI from Equation (1) and found no systematic PRI differences between the trees or the shoots of the same class (sunlit or shaded). Hence, to obtain the typical daily PRI cycle for each of the two classes with minimum uncertainty, we calculated the mean value and its 90% confidence interval for measurements pooled within a window of approximately 1 h (hereafter called “pooled PRI data”). Between 36 and 82 measurements were averaged into one data point in 2014 (average number of measurements: 55), and between 60 and 180 measurements (average: 86) in 2015. The total number of acquired needle spectra was 766 in 2014 and 1550 in 2015. The measurements were performed under clear skies, where possible. Unfortunately, this was not always possible as cloudless days are a rarity in the region. When measuring under broken skies, measurements were aborted when the sun was blocked and was not recommenced before approx. 10 min after the cloud shadow had passed.

2.2. Needle Biochemical Properties

Chlorophyll and total carotenoid concentrations were sampled at the beginning of July 2015, before the measurement campaign. Three to four previous-year needles were taken from each shoot used in the measurement and frozen in liquid nitrogen until analysed in laboratory three months later. Pigments were extracted from approximately 100 mg of fresh needle material using, first, 100% acetone, followed by 80% acetone. The solutions were analysed photometrically (UV-1650PC, Shimadzu Corp., Kyoto, Japan) and pigment concentrations calculated using the equations published by Lichtenthaler [28]. The concentrations were converted to chlorophyll a and b, and total carotenoid contents on fresh needle weight basis. A total of 72 samples were analysed (three samples were taken from 24 shoots: two light conditions \times four shoots per tree \times three trees).

2.3. Shoot Chamber Data

Carbon fluxes of individual pine shoots were measured using a dynamic gas exchange measurement system consisting of chambers, sample tubing, analysers, and a control unit (Figure 1). The chambers were made from PMMA (polymethyl methacrylate) and the inner surfaces were coated with FEP (fluorinated ethylene propylene) film. Needle growth was prevented by de-budding the shoots before installing the chambers. Thus only fully-expanded previous-year needles were included. The chambers were installed in top whorls on topmost, fully-exposed shoots, and were pointing towards the south. A small fan was mixing air inside the chambers. One shoot chamber was used in 2014 and two chambers in 2015. One of the chambers used in 2015 contained a flattened shoot: the needles were carefully spread inside the thin chamber to avoid self-shading. Other shoots were contained in cylindrical chambers which did not deform the shoot shape.

During operation the chambers remained open and the gas concentrations were close to ambient. The chambers closed automatically 48 to 72 times per day for 1.5 to 3 min for determining the gas exchange rates of the shoots enclosed inside the chamber. During measurements, sample air flow (with a flow rate of 3–4 clpm) was drawn to an infra-red gas analyser (LI-840A, LI-COR, Lincoln, NE, USA) which recorded the CO_2 and H_2O concentration change during each closure with 5-s interval. Photosynthetic photon flux density (PPFD) and temperature inside the chamber were recorded with the same frequency, using an LI-190 quantum sensor (LI-COR, Lincoln, NE, USA) and a t-type thermocouple or PT100 resistance thermometer, respectively. The needle areas were determined after

the measurement period for calculating the exchange rates per needle area units. A detailed description of the system and gas-exchange rate calculation can be found in [29,30].



Figure 1. Shoot chamber with (a) undeformed, and (b) flattened shoots in the open position.

The measurements were used to determine shoot net assimilation (A) in units of grams of CO_2 . Nighttime measurements were used to determine the shoot respiration (R). We used nighttime measurements to determine the relationship between temperature and respiration (Appendix A). Based on the high dispersion of the relationship, we assumed the simplest linear relationship between temperature and respiration and calculated shoot respiration for the time of each measurement. Added respiration to net assimilation yielded the shoot photosynthetic assimilation:

$$P = A + R \quad (2)$$

Finally, we calculated the shoot LUE, ϵ , as:

$$\epsilon = P/\text{PPFD} \quad (3)$$

where PPFD is measured in $\mu\text{mol m}^{-2} \text{s}^{-1}$. Due to the natural variation in shoot structure (e.g., in the ratio of projected to total needle area for different illumination angles, [31]), between the flat and cylindrical chambers, the results were not directly comparable between the shoots with different surface areas. However, as we were only interested of the correlations of P and ϵ with PRI, an absolute scale is not required. Hence, we normalized P and ϵ by their maximum daily values.

To achieve compatibility with needle PRI measurements (i.e., to obtain a sunlit shoot data value for the time of each needle PRI data point), the data were first visually filtered for the presence of clouds using the PPFD values. We averaged data from all days during which needle PRI was measured for each campaign (i.e., excluding the days with heavy cloud cover) were averaged, and resampled to a regular grid and smoothed with a Savitzky-Golay filter. Thus, we obtained the typical mid-summer daily cycles for the sunlit shoot normalised photosynthetic assimilation P and light use efficiency ϵ for the two campaigns.

2.4. Canopy Flux Data

The data available from SMEAR II [32] were used for two purposes: to investigate the effect of photosynthetic downregulation as indicated by daily needle PRI cycle on the landscape level, and to search for correlations between photosynthetic downregulation and meteorological conditions affecting the shoot. Hence, we retrieved from SmartSMEAR (<http://avaa.tdata.fi/web/smart/smea>) data for Gross Primary Production (GPP) [33], top-of-canopy downwelling and upwelling PPFD at 67 m above ground, and various meteorological variables at 16.8 m above ground (relative humidity, temperature, water vapour concentration). In 2015, the station recorded canopy PRI with a two-channel radiation sensor (field of view for downward sensor 45° , instrument SKR 1800, Skye Instruments, Powys, UK) from 31 m above ground. GPP was available at 30-min intervals, and all other data were available at one-minute resolution. We calculated an additional variable not available in SmartSMEAR:

the vegetation canopy LUE, ε_{can} , as the ratio of GPP to absorbed PPFD; the latter was obtained as the difference between the incident and reflected fluxes. Similarly to shoot chamber data, a typical daily curve was constructed for each campaign from the data recorded on days of needle PRI measurements.

3. Results

The needle PRI values showed considerable variation during the measurement campaigns (Figure 2). The measurement campaigns were characterized by mostly broken skies typical of the region with measurements concentrated on the days with smaller variations incident PPFD. PRI varied between 0.010 and 0.045 in 2014, and between -0.011 and 0.025 in 2015.

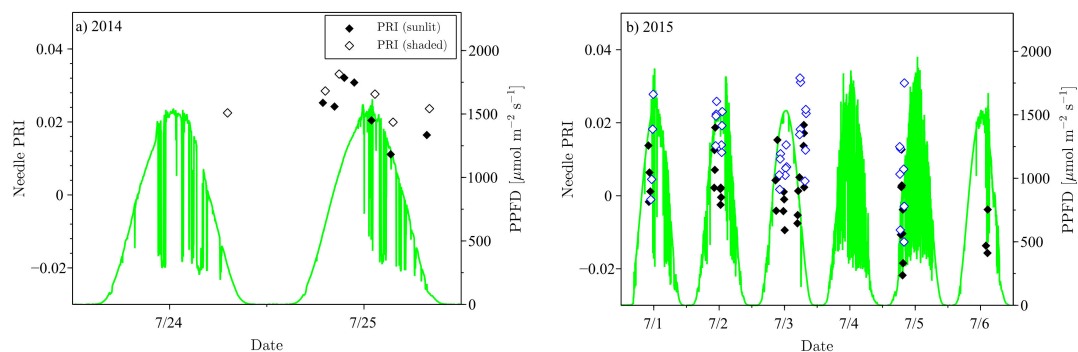


Figure 2. Needle PRI measurements (symbols, left axes) and top-of-canopy PPFD (right axes) during the two measurement campaigns in (a) 2014 and (b) 2015. On the horizontal axes, date numbers are located at the local solar noon.

Needle PRI values in the pooled PRI data showed diurnal variations (Figure 3): the sunlit needle PRI values before noon are statistically significantly ($p < 0.05$) different from the afternoon minima in both campaigns. The 90% confidence interval for the mean needle PRI was 0.0060 in 2014, and 0.0078 in the 2015 campaign. The confidence interval was considerably smaller than the measured PRI ranges of 0.026 and 0.038 in 2014 and 2015, respectively. Before noon, the PRI of sunlit and shaded needles were not statistically significantly different. In the afternoon, PRI values of shaded needles exhibited different trends in the two campaigns. In 2014, shaded needle PRI decreased simultaneously with sunlit needle PRI within the 90% confidence margin (Figure 3a); in 2015, shaded needle PRI remained constant, or increased slightly, while the values for sunlit needles decreased to recover in the evening (Figure 3b). The daily PRI curve for sunlit needles loosely followed the photosynthetic assimilation P and the light use efficiency ε of sunlit shoots in 2014 (Figure 3a).

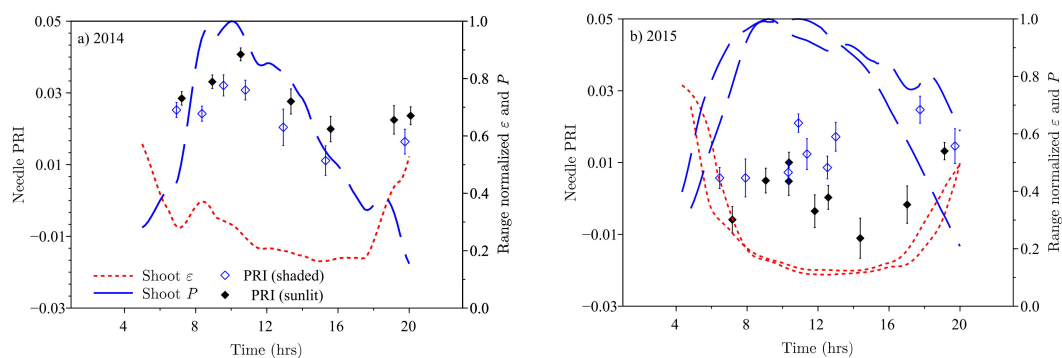


Figure 3. Diurnal variation in shaded (empty symbols) and sunlit (filled symbols) needle PRI (pooled data, left axes); and the photosynthetic assimilation P (dashed line) and the light use efficiency ε of sunlit shoots (dotted line, right axes). P and ε are normalized by their maximum daily values; (a) 2014; and (b) 2015. Error bars indicate 90% confidence limit for mean needle PRI.

The canopy LUE ε_{can} daily curve, as measured by SMEAR II (Figure 4), differed from the daily PRI curve and the sunlit shoot ε . Canopy LUE followed the PPFD time course, lacked a morning plateau, and was almost symmetrical around noon (Figure 4). The canopy PRI, PRI_{can} (Figure 4b, available only in 2015), on the other hand, had a minimum of approximately 0.005 at around 3 p.m., concurrently with the minimum in sunlit needle PRI. However, the morning increase of PRI_{can} (to the value of 0.070) took place much earlier than that of sunlit needles, before 7 a.m.

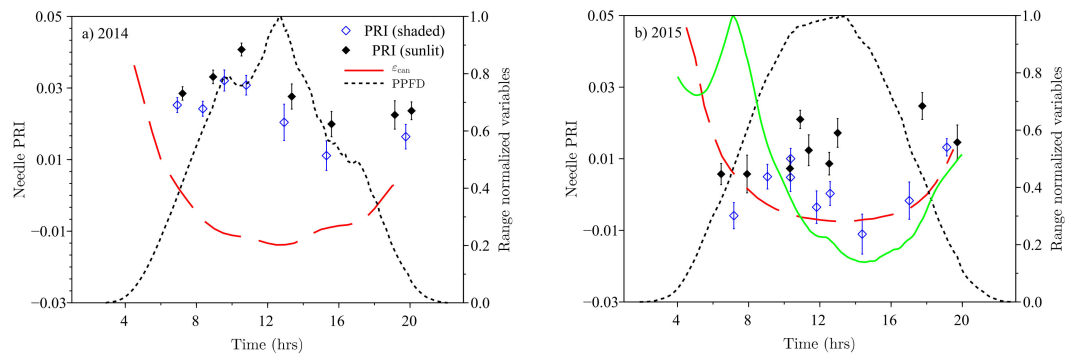


Figure 4. Diurnal variation in needle PRI (symbols, left axes) together with top-of canopy PPFD (dashed line) and the range-normalized canopy light use efficiency ε_{can} (dotted line, right axes): (a) 2014; and (b) 2015. For 2015 (b), canopy PRI data were also available (solid green line).

We found no systematic correlations between sunlit needle PRI and sunlit shoot photosynthesis on the daily scale (data not shown). However, when including only mid-day measurements using the threshold PPFD $> 1000 \mu\text{mol m}^{-2} \text{s}^{-1}$, we found significant correlations between sunlit needle PRI and the shoot LUE, ε ($p = 0.006$ and $p = 0.047$ for 2014 and 2015, respectively, Figure 5a); in 2014, when the data were obtained within 24 h, $R^2 = 0.83$. Using the same PPFD threshold, we found stronger correlations between sunlit needle PRI and the shoot photosynthetic assimilation P ($p = 0.008$ and $p = 0.001$ for 2014 and 2015, respectively, Figure 5b). We found no statistically significant correlation between needle PRI and shoot PPFD, Figure 5c): the regressions had different slopes and were statistically insignificant ($p > 0.25$).

At the canopy level (i.e., SMEAR II data), sunlit needle PRI and photosynthesis data were not correlated (data not shown) regardless of light level. However, at high light levels (PPFD $> 1000 \mu\text{mol m}^{-2} \text{s}^{-1}$), canopy and sunlit needle PRI were correlated (Figure 6a), although the correlation was not significant ($p = 0.2$). We also found systematic correlations (the same direction for all campaigns) between needle PRI and ambient air relative humidity (Figure 6b), although the correlations were not always significant ($p = 0.02$ and $p = 0.12$ for 2014 and 2015, respectively).

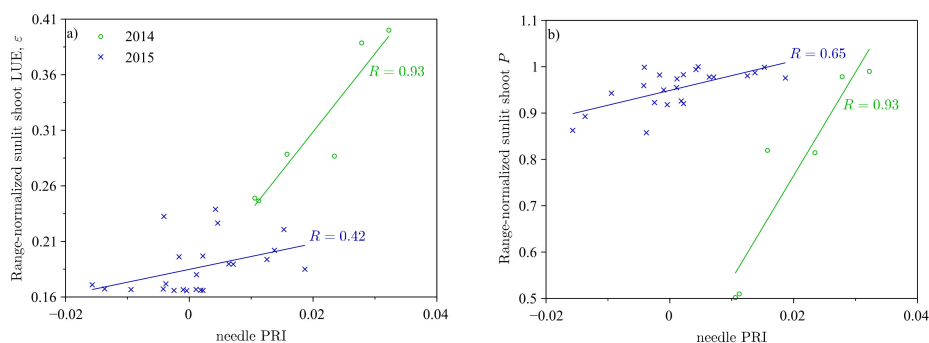


Figure 5. Cont.

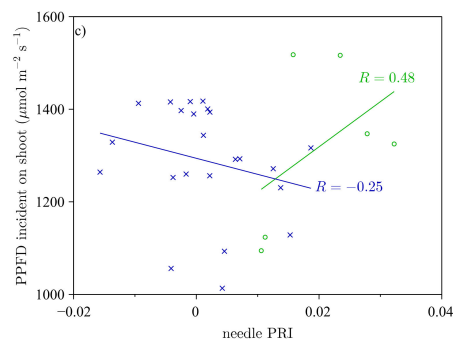


Figure 5. The correlation between needle PRI and (a) the sunlit shoot light use efficiency ϵ ; (b) photosynthetic assimilation P ; and (c) PPFD. Measurements at high light levels (PPFD > 1000 $\mu\text{mol m}^{-2} \text{s}^{-1}$); P and ϵ are normalized by their maximum value for each campaign.

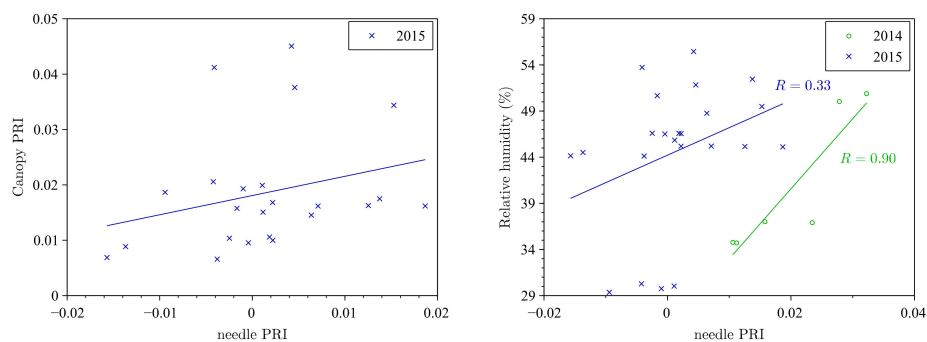


Figure 6. Correlations between sunlit needle PRI and (a) canopy PRI, and (b) relative humidity. All measurements made at high light levels (PPFD > 1000 $\mu\text{mol m}^{-2} \text{s}^{-1}$). Canopy PRI data were only available in 2015.

According to laboratory measurements, the ratio of carotenoid to chlorophyll content was somewhat larger for the sunlit than for the shaded shoots (Figure 7), but the difference was small (relative difference in $[\text{Car}]/[\text{Chl}]$ ratio: 15%) and not highly significant ($p = 0.09$, $N = 36$).

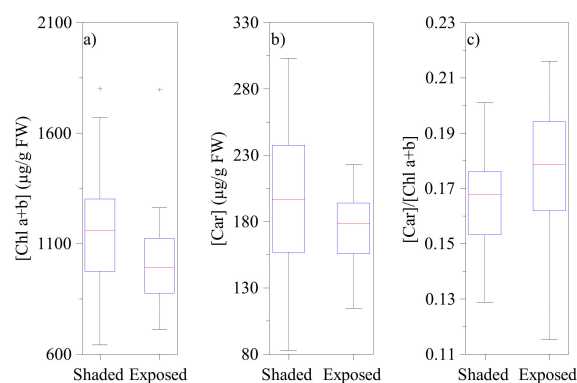


Figure 7. (a) Chlorophyll (Chl) and (b) total carotenoid (Car) concentrations; and (c) the pigment pool ratio $[\text{Car}]/[\text{Chl}]$ for the two needle classes in 2014.

4. Discussion

The strongest correlations between the sunlit shoot light use efficiency ϵ , photosynthetic assimilation P and PRI ($|R| > 0.9$, Figure 5a,b) were found during the 2014 campaign when all measurements were made within 24 h. The weakening of the correlation for the multiday 2015

campaign were possibly caused by the multi-day average curve for ϵ to cope with clouds and temporal matching of the measurements. The sunlit needle PRI was more strongly correlated with P than with ϵ (Figure 5b): lower PRI indicated a lower P . Furthermore, during the short campaign of 2015, P varied up to 50% of its daily range during the high PPFD period and, the needle PRI could explain almost all of this variation ($R^2 = 0.86$). Together with the lack of correlation between mid-day sunlit needle PRI and PPFD (Figure 5b), this result indicates that daily variations in needle PRI can indeed be used to trace shoot-level photosynthetic activity. Although these correlations only held when $PPFD > 1000 \mu\text{mol m}^{-2} \text{s}^{-1}$, these high light conditions correspond approximately to between 8 a.m. and 5 p.m. local time and include most remote sensing opportunities.

Sunlit needle PRI was only weakly ($R = 0.26$) correlated with the PRI value measured above the canopy (Figure 6a) despite the apparently similar diurnal cycles of canopy and needle PRI in the afternoon (Figure 4c) and the coincidence of their daily minimum at approximately 3 p.m. Contrastingly, canopy PRI decreases continuously after 7 a.m., while needle PRI has a maximum around 11 a.m. Additionally, shaded needles also contribute to canopy PRI. These factors, however, cannot account for the differences in the ranges of canopy (~ 0.07) and sunlit needle (~ 0.02) PRI. The direct effects of canopy structure on PRI can be quantified using the harmonic means of needle albedos at the two wavelengths (531 and 570 nm) and the photon recollision probability inside the canopy [34]. Pine needle spectral albedos at 531 and 570 nm in Hyytiälä at a similar point in the growing season were measured as 0.222 and 0.216, respectively [35]. Using the within-shoot photon recollision probability of 0.40 [36] and a between-shoot probability of 0.62 (obtained from canopy gap data measured at the site in 2014 using LAI-2000, LI-COR, Lincoln, NE, USA [37]), total within-canopy recollision probability should equal 0.77 [38]. Based on these values, canopy PRI should differ from that of a needle by a factor of 1.2—which was much less than what was measured. The remaining variation in canopy PRI can be attributed by the contribution of understory, the varying contributions of sunlit and shaded needles, and the influence of diffuse clear sky radiation on the overall canopy PRI [21]. The range of the latter could be sufficient to explain all of the variation in canopy PRI considering the range of diffuse and clear sky radiation—from nearly 100% at sunrise until a typical midsummer noon value (diffuse to total PPFD value of approx. 15% as determined by a BF3 sensor (Delta-T Devices, Cambridge, UK) in SMEAR II. To untangle the structural effects on canopy PRI, data on the spectral composition of incident radiation and the fraction of shaded foliage in the field of view of the sensor would be required. Hence, we could not corroborate a clear link between canopy and needle PRI as has been reported earlier [7,39], as more research is required to quantify this connection.

The sunlit needle PRI did not follow illumination (i.e., PPFD) for the measured Scots pine trees (Figure 4), a finding which contradicts earlier findings in other species [40,41]. According to our results, the diurnal cycle of needle PRI was a complicated one. Both the sunlit and shaded needles had the same PRI values in the morning (Figure 3). This is not surprising considering they have similar carotenoid to chlorophyll content ratios (Figure 7), which is the primary driver of needle PRI [17] and a similar canopy location. It should be noted that, contrary to other studies, the shaded needles measured by us were sampled from the topmost canopy layer with a high fraction of the visible sky. They differed from sunlit needles only by receiving less direct sunlight before and at noon. Needle PRI increased slightly before noon until 11 a.m., after which the PRI of sunlit needles decreased to the daily minimum value at approx. 3 p.m. Correlation with shoot photosynthesis (Figure 5) corroborates that the PRI decrease is indeed caused by biochemical changes leading to photosynthetic downregulation. By 8 p.m., the PRI values of both sunlit and shaded shoots had recovered to their morning values.

Unfortunately, clear days suitable for leaf-level diurnal measurements are hard to achieve in many regions. Leaf-level PRI measurements are laborious and need to be carried out manually. It could be argued that the limited number of successful measurement campaigns limits the generality of the daily needle PRI curves presented here. The measurements have also limited spatial coverage due to the difficulty in accessing multiple fully grown tree crowns. However, a lack of a needle PRI

recession before noon has been confirmed for the same area from carefully-corrected airborne imaging spectroscopy data [22].

We found a strong and significant correlation between sunlit needle PRI and relative humidity (Figure 6b) in 2014, but in 2015 the correlation was not significant ($p > 0.1$). Under high light conditions, relative humidity and sunlit shoot downregulation were significantly correlated ($0.1 < R^2 < 0.5$, $p < 0.01$, data not shown). Unfortunately, the spatial and temporal limitations in sampling mentioned above make it impossible to determine the mechanistic causes of the PRI variations. The strong correlation may indicate a co-variation with some environmental parameter (e.g., solar irradiance) and need not indicate a functional dependence.

To integrate the temporally-sparse PRI measurements provided by remote sensing satellites to daily and seasonal photosynthesis, it is critical to fully understand the processes involved in creating the observed temporal changes. The uncoupling of needle PRI and PPFD depend on, for example, how photoassimilates are used in relation to absorbed radiative energy, and the role of sinks in the relationship between photosynthetic assimilation and water transport. Determining the normal diurnal processes would clarify the causes of afternoon downregulation, and enable detection of deviations from the normal behaviour. The diurnal cycle of PRI is likely to be different for different species growing in different climatic conditions. An alternative would be to study this phenomenon under controlled conditions (following Alonso et al. [19]), but this is difficult for fully-grown trees and would inevitably exclude some environmental factors.

Our study supports the finding that PRI is correlated with midday LUE and photosynthesis in mid-summer conditions under high light conditions similar to those on cloudless days during remote sensing satellite overpasses. However, before this index can be applied routinely, several important complications need to be overcome. The effect of within-canopy shadowing must be accounted for [21], and correction for illumination geometry may remove apparent PRI variations. For the Hyytiälä site and midsummer conditions, it is known that a variation of canopy PRI with the shadow fraction (the fraction of shaded foliage in the field of view of a remote sensor) does not necessarily indicate a variation of leaf (needle) PRI with PPFD [22]. Airborne imaging spectroscopy data acquired before noon, and after correction the spectral composition of light incident on sunlit and shaded foliage, contained no difference in sunlit and shaded needle PRI. Indeed, according to the measurements reported here, a PRI gradient with PPFD is only expected to develop at around noon in a boreal conifer forest, contrary to what has been reported for other species (e.g., [19]). To apply the correction for the spectral composition of incident light, at least the amount of sunlit foliage in the field of view of the sensor is required [42] and, preferably, also the dependence of PRI on this fraction [22,43]. Unfortunately, this information was not available for the canopy PRI sensor. Further, in a relatively sparse boreal forest, it is also important to take into account the influence of the understory and lower canopy branches [8] as, in midsummer, the understory may contribute up to 40% of the reflected signal in the green spectral region [44]. With appropriate canopy reflectance models, this information can also be retrieved from spectral reflectance data.

We have demonstrated that optical detection of the status of the xanthophyll cycle is, indeed, a promising tool for monitoring the LUE of conifer needles and shoots. It can be applied from a remote sensing platform to improve the mapping of carbon sequestration by vegetation on a global scale. The measurements described in this paper can be used to determine the typical daily curves for needle PRI, establish the dependence of needle LUE on environmental conditions and photosynthetic history, and improving the currently existing techniques for remote measurement of carbon sequestration. After quantifying and understanding the phenomena causing the daily needle PRI curve, we can establish physical models for interpreting the signals measured by future hyperspectral satellites.

5. Conclusions

We found that during high irradiance conditions (clear sky around midday), the needle PRI of fully-grown Scots pine trees was correlated with LUE, but not with PPFD. This supports the use

of PRI as an indicator of photosynthetic activity providing information complementary to incident radiation flux and leaf conditions. The photosynthetic downregulation measured by shoot chambers in the afternoon was successfully reflected by needle PRI. Canopy PRI measured from a tower had an asymmetric daily cycle with a minimum in the afternoon similar to these of needle PRI and shoot photosynthesis. The afternoon downregulation in PRI present during the campaigns is not normally present at typical remote sensing satellite overpasses at 9–11 a.m. local time. Hence, the satellite measurements may not be representative of daily averaged LUE and additional data is required to scale the instantaneous remote measurements to longer (diurnal, seasonal) time scales. We suggest that for the successful mapping of boreal forest productivity from space, the mechanisms creating daily PRI cycles at both needle and canopy levels should be quantified and modelled.

Author Contributions: Conceptualization and methods: M.M.; leaf-level measurements: R.H.-C., V.P., and V.M.; shoot- and canopy-level measurements: J.A., J.B., and C.J.N.; and analysis: M.M.

Funding: The work was supported by Academy of Finland (266152, 272989, and 202633); Finnish Centre of Excellence in Atmospheric Sciences (Academy of Finland grant 272041); ICOS ERIC; Horizon2020 (ACTRIS, eLTER).

Acknowledgments: We acknowledge Albert Porcar-Castell for his supervision of the Skye PRI sensor and Janne Levula for overall assistance with shoot chamber measurements and Skye PRI sensor setup at SMEAR II. Carbon exchange and meteorological data were provided by the Station for Measuring Ecosystem—Atmosphere Relations (SMEAR).

Conflicts of Interest: The authors declare no conflict of interest.

Appendix A

Shoot net assimilation was determined from shoot chamber measurements in units of grams of CO₂ and normalized by shoot total needle area [29] (Figure A1). We fitted a linear relationship between temperature and assimilation to nighttime measurements (PPFD < 7 μmol m⁻² s⁻¹, Figure A2) to obtain the respiration *R* in Equation (2).

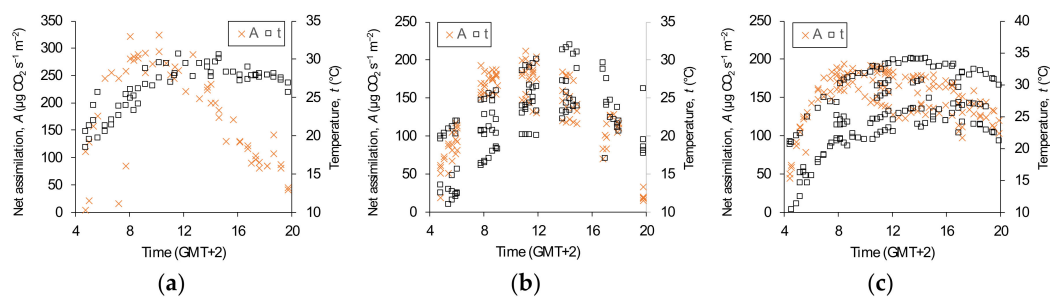


Figure A1. Daytime values of the shoot net photosynthetic assimilation *A* under full sunlight during the measurement campaigns (crosses, left axis) and the corresponding shoot chamber temperature (right axis, squares) for (a) 2014; (b) 2015 (flattened shoot); and (c) 2015 (undeformed shoot).

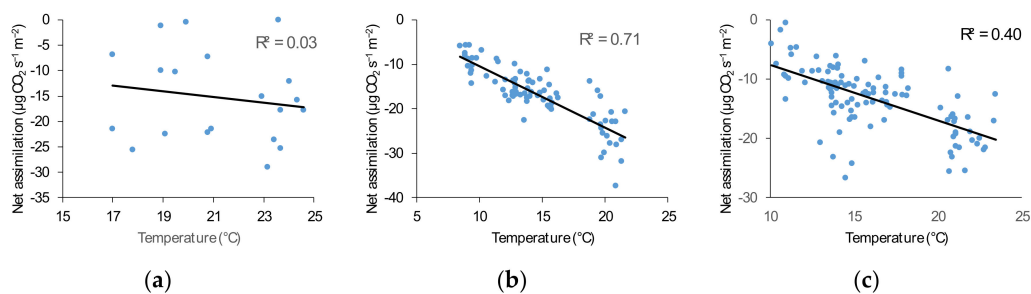


Figure A2. Nighttime correlations between shoot net photosynthetic assimilation and shoot chamber temperature for (a) 2014; (b) 2015 (flattened shoot); and (c) 2015 (undeformed shoot).

References

1. Huete, A.; Ponce-Campos, G.; Zhang, Y.; Restrepo-Coupe, N.; Ma, X.; Moran, M. Monitoring photosynthesis from space. In *Land Resources Monitoring, Modeling, and Mapping with Remote Sensing*; Remote Sensing Handbook; CRC Press: Boca Raton, FL, USA, 2015; pp. 3–22.
2. Schimel, D.; Pavlick, R.; Fisher, J.B.; Asner, G.P.; Saatchi, S.; Townsend, P.; Miller, C.; Frankenberg, C.; Hibbard, K.; Cox, P. Observing terrestrial ecosystems and the carbon cycle from space. *Global Chang. Biol.* **2015**, *21*, 1762–1776. [[CrossRef](#)] [[PubMed](#)]
3. Coops, N.C.; Hilker, T.; Hall, F.G.; Nichol, C.J.; Drolet, G.G. Estimation of light-use efficiency of terrestrial ecosystems from space: A status report. *BioScience* **2010**, *60*, 788–797. [[CrossRef](#)]
4. Grace, J.; Nichol, C.; Disney, M.; Lewis, P.; Quaife, T.; Bowyer, P. Can we measure terrestrial photosynthesis from space directly, using spectral reflectance and fluorescence? *Global Chang. Biol.* **2007**, *13*, 1484–1497. [[CrossRef](#)]
5. Gamon, J.; Peñuelas, J.; Field, C. A narrow-waveband spectral index that tracks diurnal changes in photosynthetic efficiency. *Remote Sens. Environ.* **1992**, *44*, 35–44. [[CrossRef](#)]
6. Drusch, M.; Moreno, J.; Bello, U.D.; Franco, R.; Goulas, Y.; Huth, A.; Kraft, S.; Middleton, E.M.; Miglietta, F.; Mohammed, G.; et al. The fluorescence explorer mission concept-esa's earth explorer 8. *IEEE Trans. Geosci. Remote Sci.* **2016**, *PP*, 1–12. [[CrossRef](#)]
7. Garbulsky, M.F.; Peñuelas, J.; Gamon, J.; Inoue, Y.; Filella, I. The photochemical reflectance index (PRI) and the remote sensing of leaf, canopy and ecosystem radiation use efficiencies A review and meta-analysis. *Remote Sens. Environ.* **2011**, *115*, 281–297. [[CrossRef](#)]
8. Peñuelas, J.; Garbulsky, M.F.; Filella, I. Photochemical reflectance index (PRI) and remote sensing of plant CO₂ uptake. *New Phytol.* **2011**, *191*, 596–599. [[CrossRef](#)] [[PubMed](#)]
9. Middleton, E.M.; Huemmrich, K.F.; Landis, D.R.; Black, T.A.; Barr, A.G.; McCaughey, J.H. Photosynthetic efficiency of northern forest ecosystems using a MODIS-derived Photochemical Reflectance Index (PRI). *Remote Sens. Environ.* **2016**, *187*, 345–366. [[CrossRef](#)]
10. Ulsig, L.; Nichol, C.J.; Huemmrich, K.F.; Landis, D.R.; Middleton, E.M.; Lyapustin, A.I.; Mammarella, I.; Levula, J.; Porcar-Castell, A. Detecting inter-annual variations in the phenology of evergreen conifers using long-term modis vegetation index time series. *Remote Sens.* **2017**, *9*, 49. [[CrossRef](#)]
11. Drolet, G.G.; Middleton, E.M.; Huemmrich, K.F.; Hall, F.G.; Amiro, B.D.; Barr, A.G.; Black, T.A.; McCaughey, J.H.; Margolis, H.A. Regional mapping of gross light-use efficiency using MODIS spectral indices. *Remote Sens. Environ.* **2008**, *112*, 3064–3078. [[CrossRef](#)]
12. Goerner, A.; Reichstein, M.; Tomelleri, E.; Hanan, N.; Rambal, S.; Papale, D.; Dragoni, D.; Schimullius, C. Remote sensing of ecosystem light use efficiency with MODIS-based PRI. *Biogeosciences* **2011**, *8*, 189–202. [[CrossRef](#)]
13. Lee, C.M.; Cable, M.L.; Hook, S.J.; Green, R.O.; Ustin, S.L.; Mandl, D.J.; Middleton, E.M. An introduction to the NASA Hyperspectral InfraRed Imager (HyspIRI) mission and preparatory activities. *Remote Sens. Environ.* **2015**, *167*, 6–19. [[CrossRef](#)]
14. Gamon, J.A.; Berry, J.A. Facultative and constitutive pigment effects on the Photochemical Reflectance Index (PRI) in sun and shade conifer needles. *Isr. J. Plant Sci.* **2012**, *60*, 85–95. [[CrossRef](#)]
15. Porcar-Castell, A.; Tyystjärvi, E.; Atherton, J.; van der Tol, C.; Flexas, J.; Pfundel, E.E.; Moreno, J.; Frankenberg, C.; Berry, J.A. Linking chlorophyll a fluorescence to photosynthesis for remote sensing applications: Mechanisms and challenges. *J. Exp. Bot.* **2014**, *65*, 4065–4095. [[CrossRef](#)] [[PubMed](#)]
16. Wong, C.Y.; Gamon, J.A. Three causes of variation in the photochemical reflectance index (PRI) in evergreen conifers. *New Phytol.* **2015**, *206*, 187–195. [[CrossRef](#)] [[PubMed](#)]
17. Garrity, S.R.; Eitel, J.U.H.; Vierling, L.A. Disentangling the relationships between plant pigments and the photochemical reflectance index reveals a new approach for remote estimation of carotenoid content. *Remote Sens. Environ.* **2011**, *115*, 628–635. [[CrossRef](#)]
18. Fréchette, E.; Chang, C.Y.-Y.; Ensminger, I. Photoperiod and temperature constraints on the relationship between the photochemical reflectance index and the light use efficiency of photosynthesis in *Pinus strobus*. *Tree Physiol.* **2016**, *36*, 311–324. [[CrossRef](#)] [[PubMed](#)]

19. Alonso, L.; Van Wittenberghe, S.; Amorós-López, J.; Vila-Francés, J.; Gómez-Chova, L.; Moreno, J. Diurnal cycle relationships between passive fluorescence, PRI and NPQ of vegetation in a controlled stress experiment. *Remote Sens.* **2017**, *9*, 770. [[CrossRef](#)]
20. Galvão, L.S.; Breunig, F.M.; Santos, J.R.D.; de Moura, Y.M. View-illumination effects on hyperspectral vegetation indices in the Amazonian tropical forest. *Int. J. Appl. Earth Obs. Geoinf.* **2013**, *21*, 291–300. [[CrossRef](#)]
21. Möttus, M.; Takala, T.L.H.; Stenberg, P.; Knyazikhin, Y.; Yang, B.; Nilson, T. Diffuse sky radiation influences the relationship between canopy PRI and shadow fraction. *ISPRS J. Photogramm. Remote Sens.* **2015**, *105*, 54–60. [[CrossRef](#)]
22. Takala, T.L.H.; Möttus, M. Spatial variation of canopy PRI with shadow fraction caused by leaf-level irradiation conditions. *Remote Sens. Environ.* **2016**, *182*, 99–112. [[CrossRef](#)]
23. Damm, A.; Guanter, L.; Verhoef, W.; Schläpfer, D.; Garbari, S.; Schaepman, M.E. Impact of varying irradiance on vegetation indices and chlorophyll fluorescence derived from spectroscopy data. *Remote Sens. Environ.* **2015**, *156*, 202–215. [[CrossRef](#)]
24. Gitelson, A.A.; Gamon, J.A.; Solovchenko, A. Multiple drivers of seasonal change in PRI: Implications for photosynthesis 2. Stand level. *Remote Sens. Environ.* **2017**, *190*, 198–206. [[CrossRef](#)]
25. Merlier, E.; Hmimina, G.; Dufrêne, E.; Soudani, K. Explaining the variability of the photochemical reflectance index (PRI) at the canopy-scale: Disentangling the effects of phenological and physiological changes. *J. Photochem. Photobiol. B Biol.* **2015**, *151*, 161–171. [[CrossRef](#)] [[PubMed](#)]
26. Kolari, P.; Chan, T.; Porcar-Castell, A.; Bäck, J.; Nikinmaa, E.; Juurola, E. Field and controlled environment measurements show strong seasonal acclimation in photosynthesis and respiration potential in boreal Scots pine. *Front. Plant Sci.* **2014**, *5*, 717. [[CrossRef](#)] [[PubMed](#)]
27. Ilvesniemi, H.; Levula, J.; Ojansuu, R.; Kolari, P.; Kulmala, L.; Pumpanen, J.; Launiainen, S.; Vesala, T.; Nikinmaa, E. Long-term measurements of the carbon balance of a boreal Scots pine dominated forest ecosystem. *Boreal Environ. Res.* **2009**, *14*, 731–753.
28. Lichtenthaler, H.K. Chlorophylls and carotenoids: Pigments of photosynthetic biomembranes. *Methods Enzymol.* **1987**, *148*, 350–382. [[CrossRef](#)]
29. Kolari, P.; Lappalainen, H.K.; Hänninen, H.; Hari, P. Relationship between temperature and the seasonal course of photosynthesis in Scots pine at northern timberline and in southern boreal zone. *Tellus B* **2007**, *59*, 542–552. [[CrossRef](#)]
30. Kolari, P.; Bäck, J.; Taipale, R.; Ruuskanen, T.M.; Kajos, M.K.; Rinne, J.; Kulmala, M.; Hari, P. Evaluation of accuracy in measurements of VOC emissions with dynamic chamber system. *Atmos. Environ.* **2012**, *62*, 344–351. [[CrossRef](#)]
31. Smolander, H.; Stenberg, P.; Linder, S. Dependence of light interception efficiency of Scots pine shoots on structural parameters. *Tree Physiol.* **1994**, *14*, 971–980. [[CrossRef](#)] [[PubMed](#)]
32. Hari, P.; Nikinmaa, E.; Pohja, T.; Siivola, E.; Bäck, J.; Vesala, T.; Kulmala, M. Station for measuring ecosystem-atmosphere relations: SMEAR. In *Physical and Physiological Forest Ecology*; Springer: Berlin, Germany, 2013; pp. 471–487.
33. Kolari, P.; Kulmala, L.; Pumpanen, J.; Launiainen, S.; Ilvesniemi, H.; Hari, P.; Nikinmaa, E. CO₂ exchange and component CO₂ fluxes of a boreal Scots pine forest. *Boreal Environ. Res.* **2009**, *14*, 761–783.
34. Möttus, M.; Rautiainen, M. Scaling PRI between coniferous canopy structures. *IEEE J. Sel. Top. Appl. Earth Obs. Remote Sens.* **2013**, *6*, 708–714. [[CrossRef](#)]
35. Lukeš, P.; Stenberg, P.; Rautiainen, M.; Möttus, M.; Vanhatalo, K.M. Optical properties of leaves and needles for boreal tree species in Europe. *Remote Sens. Lett.* **2013**, *4*, 667–676. [[CrossRef](#)]
36. Stenberg, P.; Palmroth, S.; Bond, B.J.; Sprugel, D.G.; Smolander, H. Shoot structure and photosynthetic efficiency along the light gradient in a Scots pine canopy. *Tree Physiol.* **2001**, *21*, 805–814. [[CrossRef](#)] [[PubMed](#)]
37. Stenberg, P. Simple analytical formula for calculating average photon recollision probability in vegetation canopies. *Remote Sens. Environ.* **2007**, *109*, 221–224. [[CrossRef](#)]
38. Smolander, S.; Stenberg, P. Simple parameterizations of the radiation budget of uniform broadleaved and coniferous canopies. *Remote Sens. Environ.* **2005**, *94*, 355–363. [[CrossRef](#)]

39. Gamon, J.A.; Kovalchuck, O.; Wong, C.Y.S.; Harris, A.; Garrity, S.R. Monitoring seasonal and diurnal changes in photosynthetic pigments with automated PRI and NDVI sensors. *Biogeosciences* **2015**, *12*, 4149–4159. [[CrossRef](#)]
40. Evain, S.; Flexas, J.; Moya, I. A new instrument for passive remote sensing: 2. Measurement of leaf and canopy reflectance changes at 531 nm and their relationship with photosynthesis and chlorophyll fluorescence. *Remote Sens. Environ.* **2004**, *91*, 175–185. [[CrossRef](#)]
41. Gamon, J.A.; Bond, B. Effects of irradiance and photosynthetic downregulation on the photochemical reflectance index in Douglas-fir and ponderosa pine. *Remote Sens. Environ.* **2013**, *135*, 141–149. [[CrossRef](#)]
42. Hernández-Clemente, R.; Kolari, P.; Porcar-Castell, A.; Korhonen, L.; Möttus, M. Tracking the seasonal dynamics of boreal forest photosynthesis using EO-1 Hyperion reflectance: Sensitivity to structural and illumination effects. *IEEE Trans. Geosci. Remote Sci.* **2016**, *54*, 5105–5116. [[CrossRef](#)]
43. Markiet, V.; Hernández-Clemente, R.; Möttus, M. Spectral similarity and PRI variations for a boreal forest stand using multi-angular airborne imagery. *Remote Sens.* **2017**, *9*, 1005. [[CrossRef](#)]
44. Rautiainen, M.; Lukeš, P. Spectral contribution of understory to forest reflectance in a boreal site: An analysis of EO-1 Hyperion data. *Remote Sens. Environ.* **2015**, *171*, 98–104. [[CrossRef](#)]



© 2018 by the authors. Licensee MDPI, Basel, Switzerland. This article is an open access article distributed under the terms and conditions of the Creative Commons Attribution (CC BY) license (<http://creativecommons.org/licenses/by/4.0/>).